Colloidal Particles: Crystals, Glasses, and Gels

Peter J. Lu (陸述義) and David A. Weitz

Department of Physics and School of Engineering and Applied Sciences, Harvard University, Cambridge, Massachusetts 02138; email: plu@fas.harvard.edu, weitz@seas.harvard.edu

Annu. Rev. Condens. Matter Phys. 2013. 4:217–33

First published online as a Review in Advance on January 16, 2013

The *Annual Review of Condensed Matter Physics* is online at conmatphys.annualreviews.org

This article's doi:
10.1146/annurev-conmatphys-030212-184213

Keywords

fluid, jamming, confocal microscopy, gelation, spinodal decomposition, phase separation, defects, indentation, phase behavior, nucleation and growth, fractals, clusters, dynamical heterogeneity

Abstract

Colloidal particles are microscopic solid particles suspended in a fluid. Colloids are small enough that thermal energy drives their dynamics and ensures equilibration with the suspending fluid; they are also large enough that their positions and motions can be measured precisely using optical methods, such as light scattering and laser-scanning confocal fluorescence microscopy. Colloidal suspensions are a powerful model system for the study of other phenomena in condensed matter physics, where the collective phase behavior of the solid particles mimics that of other condensed systems. We review three classes of interacting colloidal particles, crystals, glasses, and gels, each of which represents fascinating properties of colloidal particles as well as a model for more general types of materials and their behavior.

1. INTRODUCTION

Colloidal particles are small solid particles that are suspended in a fluid phase. Their size range is typically between ~10 nm and several microns. This makes them small enough to be suspended in the fluid by thermal motion, provided the buoyancy mismatch between the particles and the fluid is not too large. Colloidal suspensions are very important technologically: They allow solid particles to flow like a fluid. They are used in many different applications, from paints, inks, and other coatings to critical diagnostic tests. They can be fabricated with exquisite precision; it is possible to create colloidal particles with size polydispersity of less than 3%, as measured as a standard deviation of the distribution of the particle radii. Moreover, through control of their interfacial properties, the interparticle interactions between the colloids can be tuned precisely. The strength of the potential can be varied from strongly repulsive to strongly attractive, and can include both repulsive and attractive parts; moreover, the range of the interaction potential can be varied from distances two orders of magnitude smaller than the particle diameter to distances larger than the particle itself. However, colloidal particles are intrinsically only kinetically stable, as they consist of a dispersed solid phase, whose energy would be in a lower state were they not dispersed but instead a simple solid. Thus, in all cases, there must be some repulsive energy barrier to prevent irreversible aggregation of the particles, typically due to van der Waals attractions.

The precise control of their size and interaction potential makes colloidal particles a very valuable model system for the study of many different types of behavior. In this case, it is typically the properties of the particles themselves that are of interest. The fluid serves to thermalize the particles, ensuring that they can equilibrate and sample all of phase space. It is the phase behavior of the particles themselves that makes the study of colloidal suspensions so interesting. For example, one particularly intriguing example is the use of colloidal particles to model more traditional atomic or molecular solids. The phase behavior of the colloidal particles is similar to that observed in atomic or molecular samples. However, for colloidal samples, it is possible to visualize each particle and follow its motion in both space and time, with techniques such as laser-scanning confocal fluorescence microscopy. This provides a completely different type of information about the system and represents a means of probing dynamics of the phase behavior at the single-particle level, which is not in general possible with atomic and molecular systems. This combination of properties—the ability to carefully synthesize predesigned sizes and properties and a size range large enough to probe single particles, yet small enough that thermal energy controls the particle dynamics—makes colloidal systems uniquely powerful as probes of the fundamental behavior of condensed matter systems.

In this review, we focus on the study of colloidal suspensions as model systems of collective behavior. We describe the nature of the particles that are most widely used in these studies, and then briefly review three different types of colloidal behavior: crystals, glasses, and gels.

2. SAMPLES

The use of colloidal particles as model systems is predicated in large measure by our ability to synthesize particles whose sizes are highly monodisperse and whose interparticle interactions are highly controlled. In addition, colloidal particles can be synthesized from many different materials. One of the most important features often exploited is the use of a solid material whose index of refraction is precisely matched to that of the suspending solvent. This greatly reduces the strong scattering of light that is typically observed from the particles. This allows optical techniques such as light scattering and confocal microscopy to be used to measure the behavior of the particles, thereby enhancing the experimental probes of these systems.

One of the most widely studied model systems is the hard-sphere system (1, 2), where the colloidal particles interact only through volume exclusion; this requires a very strong, repulsive interaction when the particles touch, but no interaction whatsoever when the particles are not touching. This interaction is particularly convenient to study because it has been extensively modeled through theory and simulation. Typically, the repulsive interaction does not have a range of strictly zero, but is instead usually very short ranged. One of the most widely studied systems is that of polymethylmethacrylate (PMMA) particles, sterically stabilized by a thin coating of polyhydroxystearic acid (PHSA); these particles have a very strong repulsion that extends only a few nanometers from their surface. The refractive index of these particles can be matched closely to that of the surrounding solvent by using mixtures of two or more nonaqueous solvents; furthermore, some solvent combinations have been used to match not only the refractive index, but also the density of the colloidal particles, thereby minimizing the effects of sedimentation (3, 4). Other solvent combinations have been chosen because of electrostatic behavior; even in nonaqueous solvents, these colloidal particles still may become somewhat charged, and this charging effect can result in a longer-ranged repulsive interaction. To control these effects, charge-stabilizing agents can be added to the solvent, and these agents solubilize charges both in solution and on the surface of the particles; this provides a convenient way to study the effects of charge interactions in nonpolar solvents (5) and has the advantage of increasing all the relevant length scales associated with the charges relative to atomic systems.

Another widely studied model colloidal system is charge-stabilized polystyrene latex particles. These particles interact through a screened Coulomb interaction, whose amplitude is determined by the charge on the particle surface, and whose range is determined by the screening length in the solvent (6–8). In contrast to the PMMA system, these particles cannot be index-matched too closely to the solvent and, hence, can only be studied with single-particle resolution at very low concentrations. Interaction effects become important when the range of interparticle interaction is comparable to the average interparticle separation; consequently, ensuring that the particle concentration is sufficiently low to enable visualization requires a screening length of order a few hundred nanometers. This requires very low concentrations of excess salt; as a result, these systems are often prepared with ion-exchange resin to reduce charge, and are held under an inert atmosphere, because even the CO_2 found naturally in the atmosphere can lead to excess charge in the solution (9).

3. CRYSTALLIZATION

One of the most widely studied colloidal interactions is the hard-sphere interaction, in which the colloidal particles interact solely by volume exclusion. Here, there is no long-range repulsion; instead, only a very short-range, and very large, repulsion between particles prevents them from sticking to one another. The first experimental realization of the hard-sphere system was PMMA stabilized by PHSA, a system still widely studied. The first observation of interesting behavior in this system is that the particles crystallize as their volume fraction, φ, increases, and exhibit a fluid-crystal coexistence region for $0.49 \leq \varphi \leq 0.54$ (1). This phase behavior is in excellent accord with computer simulation. Nevertheless, this is somewhat counterintuitive: With no interaction potential between the particles, their phase behavior is determined exclusively by entropy; typically, lowering the free energy through entropy leads to an increase in disorder, rather than the increased order observed for crystallization. The packing behavior of spherical particles resolves this apparent inconsistency: When the particles are strictly disordered, they pack to a maximum volume fraction determined by the value for random close packing of spheres, $\varphi_{rcp} \approx 0.64$; by contrast, when the particles order into a crystalline lattice, they can pack much more tightly, at $\varphi_c \approx 0.74$

for a face-centered cubic (fcc) lattice. Because the entropy is dominated by the number of configurations that the particles can achieve, it is controlled by the free volume, the difference in the volume fraction between the actual volume fraction and the maximum value for the particle structure. Thus, the free volume is always greater when the particles adapt a crystalline lattice than when they are packed in a random structure, and this drives crystallization for $\varphi \geq 0.49$.

Colloidal crystals traditionally have been studied using scattering methods, which provide an excellent ensemble average over large volumes of the crystal, and which are ideally suited for ordered samples where Bragg scattering or diffraction techniques can probe the properties of the order. However, in many cases, there are phenomena that are much better probed in real space, rather than with scattering. One example is the nucleation and growth process of crystallization itself (10). Because the initial crystallization occurs locally, it is much more conveniently probed by imaging the particles individually, as shown in **Figure 1**. The growth of crystals from the melt can be quantified by determining the local crystalline order parameter and by following the growing crystallites. This provides a much richer and more detailed view of the structure of the nuclei; they tend to be rather disordered, with the crystalline order difficult to discern when they are small. Moreover, the rate of nucleation seems to be significantly larger than that expected from computer simulation.

More complex colloidal crystal structures can form in mixtures of particles of different sizes, again, for example, suspensions with hard-sphere interactions. Both the packing of the binary

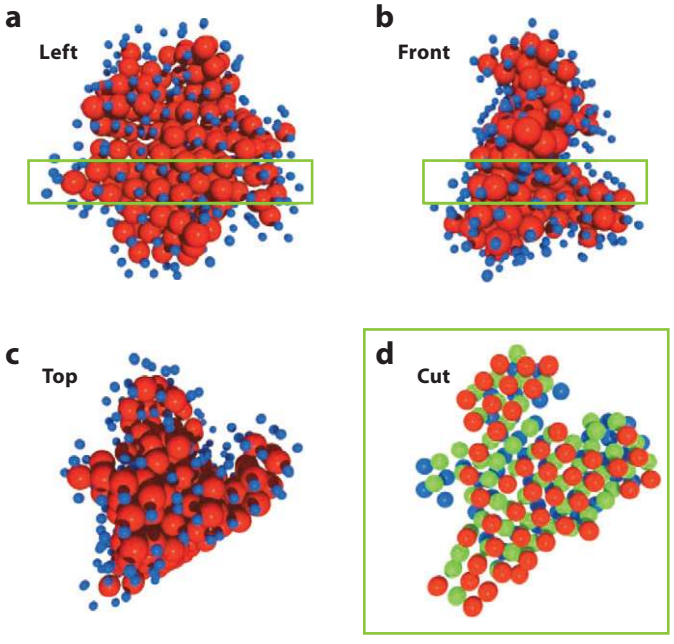

Figure 1

A snapshot of a crystallite of postcritical size in a sample with $\varphi = 0.47$ is shown from three different directions (*a–c*). The 206 red spheres represent crystal-like particles and are drawn to scale; the 243 extra blue particles share at least one crystal-like bond to a red particle but are not identified as crystal-like and are reduced in size for clarity. (*d*) A cut with a thickness of three particle layers through the crystallite, illustrating the hexagonal structure of the layers. Blue, red, and green spheres represent particles in the different layers (front to rear). This cut was taken from the region that is indicated by the green boxes in panels *a* and *b*. The particle diameter in panel *d* is reduced to improve the visibility of the second and third layers (10).

mixtures and their relative sizes determine exactly what structure is formed. An even richer array of structures can form if the particles are slightly charged (11), as this can lead to a less dense packing of the particles when crystallization does occur. Charged colloidal particles can also exhibit crystalline ordering. Here, the crystallinity is better described as the formation of a Wigner crystal, a structure that forms when the particles are highly repulsive, but constrained within the sample by the boundaries. The strong repulsion between the particles ensures that the range of φ over which crystallization is observed is much greater than that for hard spheres (12).

The ability to visualize all the particles individually in a colloidal crystal makes possible detailed investigations of the nature of defect structures (13). To accomplish this, it is necessary to form large, defect-free colloidal crystals. This is not feasible with crystals that are formed spontaneously from the melt, because the crystal structure adopted is not a perfect crystal, but is instead a mixture of fcc and hexagonally close-packed (hcp) structures; the resulting structure is a random stacking of hexagonal planes, called random-hcp (14), a mix of fcc and hcp structures that is thus not a true crystal. Therefore, to investigate the behavior of perfect crystals, it is necessary to grow the colloidal crystals on a template that forces a specific order into the sample. The most commonly used template is a square lattice, representing the 110 plane of an fcc structure. This template can be a flat surface with small holes, ~25% of the radius of the particles, arrayed on a square lattice, with the lattice constant appropriate for the colloidal sample studied (15). If the particles are slightly buoyancy mismatched, they will sediment onto the template, filling the holes and causing them to form an ordered structure, on which additional planes of the crystal can grow. Using this method, it is possible to grow nearly perfect colloidal crystals.

The perfect crystal lattice formed with this template can be used to study different phenomena that mimic the behaviors of atomic or molecular crystals. For example, if the template lattice constant is very near, but not exactly at, the value required for the colloidal crystal, the crystal will be strained as it grows and tries to transition from the imperfect lattice to a perfect one. The strain increases as the crystal thickness grows from when it is first deposited, ultimately becoming too large and forcing the creation of a stacking fault (13). The dynamics of this defect creation can be monitored directly, using either confocal microscopy or laser-diffraction microscopy (13), in which Bragg scattered light is imaged to visualize directly defects in a crystalline structure, as shown in **Figure 2**.

Defect formation can also be visualized directly when the defects are induced through deformation of the crystal, for example, via the equivalent of nanoindentation: For colloidal particles, the nanoindenter is replaced by a sharp needle whose radius of curvature is of order 25 μm (16). Interestingly, because the strain can be applied so slowly, it is possible to observe directly the thermal activation of defects; this is nearly impossible with atomic and molecular crystals, because the motion required to achieve equivalent strains is so much less, on account of the far smaller atomic unit cell.

4. GLASSES

Colloidal particles also represent an excellent model system for the study of glasses (2). When the particles interact by volume exclusion, glass-like behavior is driven exclusively by packing considerations. As φ increases, the particles become increasingly crowded by their neighbors, and structural relaxation of the particles slows dramatically; the properties of this slowing are readily studied with colloidal particles because their motion can be monitored using either scattering methods or microscopy.

A glass and a liquid are very similar in structure: Both have a disordered character, which can be described through the static structure factor, $S(q)$, where q is the scattering wave vector. The

difference between the two lies in the dynamics: A liquid undergoes structural relaxation on a much shorter timescale than does a glass. Indeed, the slowing down of the structural relaxation as a glass is approached is one of the hallmarks of the glass transition. For hard-sphere colloidal particles, this slowing down results from the crowding of the particles, which makes their structural relaxation increasingly difficult, and is well described by mode-coupling theory in an early success of the paradigm.

The slowing down of the structural relaxation of the particles upon approaching the glass transition also profoundly affects the rheology of the colloidal suspension: At low φ, the suspension is purely viscous; as φ increases, the suspension becomes viscoelastic, and over an increasing range of frequencies, it becomes elastic (17). The rheological response is also well described using a mode-coupling-theory approach. Moreover, using confocal microscopy, it is possible to visualize those regions of the sample that have not relaxed and therefore can transmit forces as solid regions (18): As the volume fraction of the glass transition is approached, the sample relaxes much more slowly, and much larger regions remain static and can therefore transmit forces as a solid. This is a very intuitive means of visualizing the nature of the glass, which directly couples structural relaxation with force transduction.

The ability to visualize the motion of the individual particles has enabled a much greater exploration of these phenomena. As the glass transition is approached, the structural relaxation becomes more and more heterogeneous (19, 20): Relaxation occurs as a result of large-scale collective motion of many particles, and the range of these relaxation events increases as the glass transition is approached, becoming larger than the sample observation size very close to the glass transition. This is a direct observation of the dynamical heterogeneities (shown in **Figure 3**) that were initially predicted through computer simulation and were observed more indirectly through scattering methods; by contrast, these can be seen directly in colloidal systems.

The motion of the colloidal particles that leads to the structural relaxation also can be observed directly when the volume fraction is further increased and the sample becomes a glass. This is best observed through the application of shear to the system (21). The combination of the shear and thermal excitations drives local structural rearrangement events called shear transformation zones (22, 23), which are directly observed by monitoring the motion of the particles; moreover, as the strain increases, these shear transformation zones increase in number and ultimately fill the whole system. They seem to spread in a coupled fashion, which may reflect elastic coupling, or, alternatively, spreading through dissipative disordering (24, 25), eventually leading to flow of the glass, as shown in **Figure 4**.

Figure 2

Laser-diffraction microscopy (LDM) technique and images. (*a*) Schematic of the LDM instrument: A laser beam is sent through a colloidal crystal. One of the diffracted beams is imaged on a screen by means of an objective and a projector lens. (*b*,*c*) LDM images of the colloidal crystal grown on the template with the ideal lattice constant $d_0 = 1.63\ \mu$m. Thick white arrows indicate dislocations. The upper left inset shows the diffraction pattern from the crystalline film; 0 indicates the transmitted beam, and a thin white arrow indicates the diffracted beam used for imaging. The upper right inset illustrates the wave vectors of the incident and diffracted beams k_0 and k, the diffraction vector $q = k - k_0$, and the corresponding reciprocal lattice vector g. In panel *b*, the diffraction vector q coincides with the reciprocal lattice vector g, and the diffracted beam intensity is maximum. In panel *c*, the sample is tilted so that q differs from g by the excitation error $s = q - g$, which gives rise to an inversion of the image contrast. (*d*–*g*) LDM images of a colloidal crystalline film grown on a stretched template with lattice constant $d_1 = 1.65\ \mu$m. Panels *d* and *e* show that using the (220) diffraction vector, which lies along the $\hat{y}$-direction, gives images of dislocations oriented in the $\hat{x}$-direction. Panels *f* and *g* show that choosing the $(\bar{2}20)$ diffraction vector, which lies along the $\hat{x}$-direction, images dislocations oriented in the $\hat{y}$-direction (13).

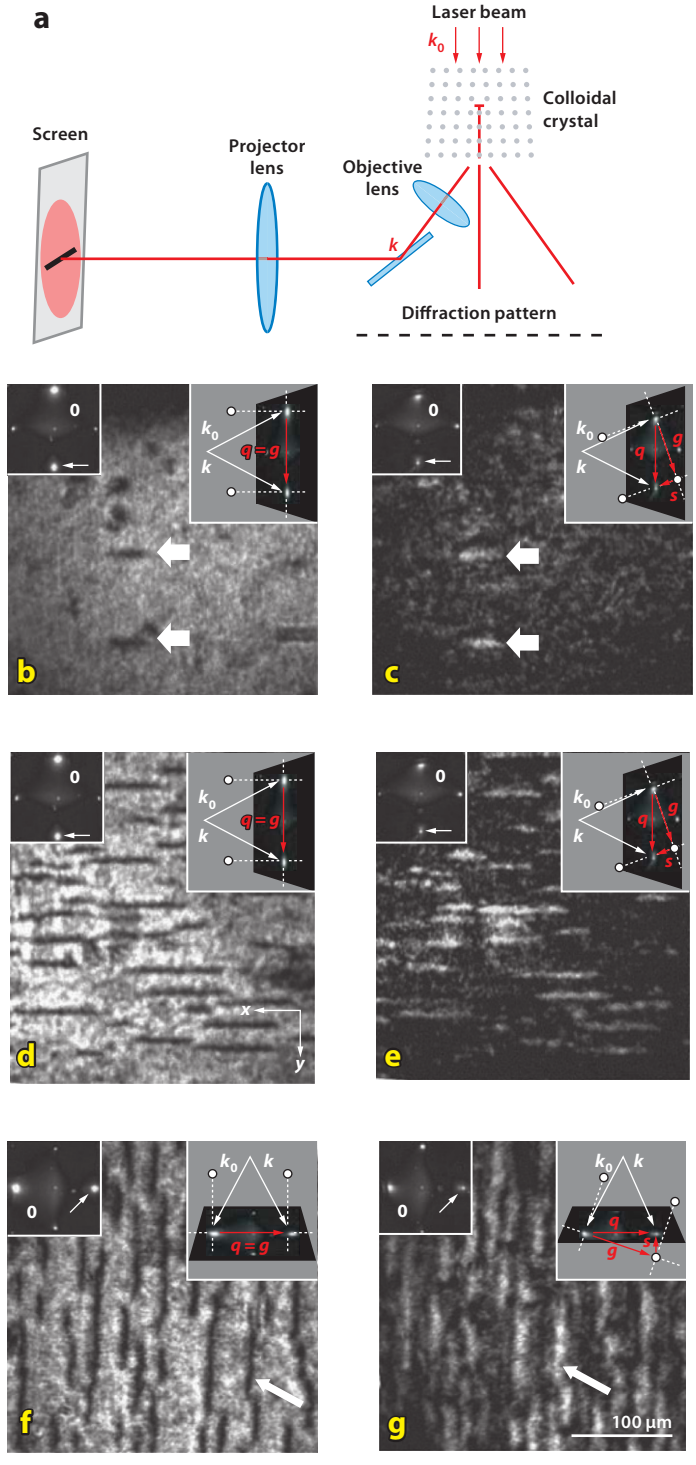

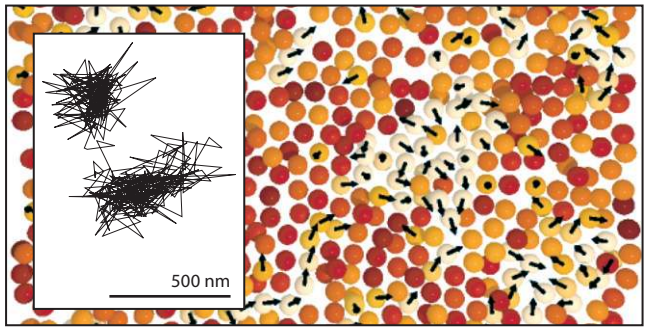

Figure 3

A cut through a three-dimensional sample, with black arrows indicating the direction of motion for particles with displacements $\Delta r > 0.2$ μm, using $\Delta t^* = 600$ s. The sample has $\varphi = 0.52$, and the cut is 2.5 μm thick ($\approx$1 layer of particles). All arrows are the same length in three dimensions, so shortened arrows indicate motion in or out of the plane. Lighter colors indicate particles with larger displacements. (*Inset*) 120-min trajectory of one particle from this sample (19).

Hard-sphere colloidal particles exhibit a very strong divergence as the glass transition is approached, as crowding very rapidly increases and prevents the structural relaxation. As a result, the increase in relaxation time occurs over a very narrow range of volume fractions. By contrast,

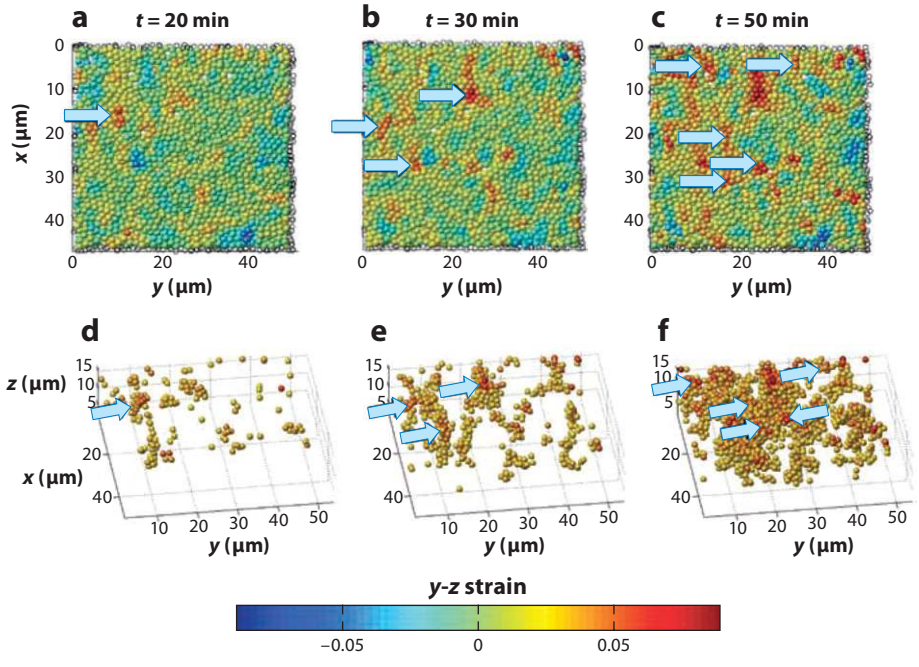

Figure 4

Strain evolution during shear. Distribution of the cumulative shear strain after 20, 30, and 50 min of shear. For each frame, blue arrows indicate shear transformation zones that have been formed in the time interval before the frame shown. Shear transformation zones appear to form a connected network at $t = 50$ min. (*a–c*) $\hat{x} - \hat{y}$ sections (5 μm thick) centered at $z = 13.5$ μm. (*d–f*) Perspective view of 16-μm-thick sections showing particles with shear strain values larger than 0.025 only (21).

deformable colloidal particles, or microgels, can be packed to higher densities, as the solvent can be squeezed out of the particles. These systems also undergo a glass transition, but do not exhibit the same strong divergence as the glass transition is approached; instead, their approach is more gradual (26). Moreover, as the microgel particles are made increasingly deformable, by decreasing their elastic modulus, the approach to the glass transition becomes correspondingly more gradual. This behavior is very similar to the approach of strong and fragile glasses to the glass transition, with the fragile glasses exhibiting a more divergent character than the strong glasses.

In addition to particles interacting only through repulsive interactions, a colloidal glass is also observed for particles that are weakly attractive (27). In this case, the glass transition occurs at a slightly higher value of φ, as weak attractive interactions cause particles to stick to their neighbors, leaving a slightly larger free volume that facilitates structural relaxation of some particles; the net result is an increase in the volume fraction of the glass transition.

5. GELS

When the attraction between colloidal particles is short ranged but strong, colloidal particles diffusing in a fluid aggregate to form clusters that have a fractal structure manifest as branched, open, tenuous networks. In fractal clusters, a small number of particles occupy a large volume of space. The behavior falls into two broad limits. When particles stick irreversibly to each other upon contact, then the only factor governing the system's behavior, and hence the morphology of the clusters, is the diffusion of particles; this is diffusion-limited cluster aggregation (DLCA), where the clusters have a low fractal dimension of 1.8 (28), as shown in **Figure 5**.

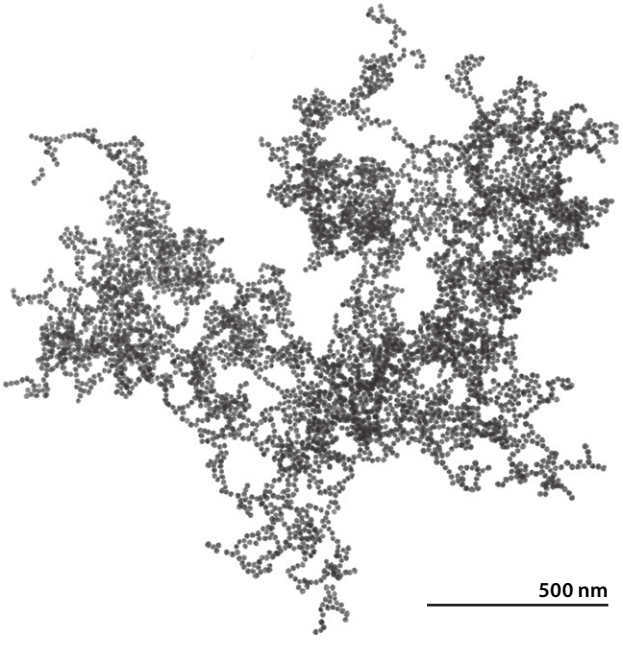

Figure 5

Transmission electron micrograph of a typical gold colloid aggregate formed by diffusion-limited cluster aggregation (DLCA), containing 4,739 gold particles (28).

By contrast, in reaction-limited cluster aggregation (RLCA), the particles must first overcome a repulsive barrier before bonding, thereby requiring multiple attempts before an interparticle bond can form (29). This behavior leads to more compact clusters with a higher fractal dimension. Interestingly, the cluster morphology in these two limits reflects the geometry of the corresponding aggregation processes themselves, incorporating the fractal dimension of the cluster trajectories that lead to their formation. Diffusing particles follow a random walk, which has a fractal dimension of two. By contrast, the multiple approaches of two particles in RLCA results in a trajectory with a fractal dimension of zero, leading to more compact clusters with higher fractal dimensions. The DLCA and RLCA paradigms are universal, independent of the nature of the material, and are seen, inter alia, in colloidal gold, silica, and polystyrene suspensions (30), as shown in **Figure 6**.

Both DLCA and RLCA are purely kinetic phenomena; dynamic particle motion, driven by diffusion, or the kinetics of chemical reactions, can account quantitatively for the rates of cluster formation and the subsequent cluster morphology (29). However, attractive and repulsive interactions in a system of particles can also lead to rich thermodynamic phase behavior, such as the formation of liquids, gases, and crystals. Whenever there is an attractive interaction, some sort of phase separation can occur, as the system minimizes its free energy by splitting into two phases, often via spinodal decomposition. When this occurs in low-φ colloidal suspensions that undergo DLCA, fractal clusters form, but these have an interparticle structure and dynamics that scale consistently in a manner observed in early-stage spinodal decomposition, provided that the fractal dimension $d_f < 1.9$ of DLCA is used in place of the $d_f = 3$ of spinodal decomposition (31), as shown in **Figure 7**.

This observation suggests a connection during cluster formation between two very general classes of phenomena: thermodynamic phase separation, particularly the spinodal decomposition that is observed in a wide range of liquid-gas systems and particle systems with attractive interactions, and the aggregation processes regarded as purely kinetic limits. Moreover, the formation of gels—spanning, arrested networks—often represents the final, arrested state of cluster aggregation, making the general connection to spinodal decomposition even more intriguing.

In the DLCA and RLCA aggregation limits, the interparticle attraction is extremely strong but very short ranged, and the particles themselves are held at very low densities. Each of these parameters—the colloid particle concentration φ (again, expressed as the fraction of the system's volume occupied by the particles), the range of the attraction ξ (expressed in units of particle radius), and the energetic strength of the attraction U (expressed in units of thermal energy k_BT)—can affect the morphology and dynamics of cluster and gel formation (3); this framework for purely attractive particles is shown in **Figure 8**. DLCA experiments represent a limit of φ and ξ going to zero, with unbreakable bonds representing energies of dozens of k_BT. Within the same framework, equilibrium liquid-gas phase separation is known from simulations to occur for particles with short-ranged attractions (again, $\xi \to 0$) when φ is well above 10%, with bond energies of a few k_BT, allowing for the rapid making and breaking of bonds that is a hallmark of an equilibrium phase-separation process.

The continuous transition between known limits of kinetic arrest (DLCA) and equilibrium thermodynamics (phase separation via spinodal decomposition) suggests a deeper connection in the factors driving the formation of gels. To investigate this possibility, several fluid and gel

Figure 6

Transmission electron micrographs of typical clusters of gold, silica, and polystyrene colloids formed by diffusion-limited and reaction-limited cluster aggregation and computer simulations. The structure of the clusters of different colloids is strikingly similar in each regime (30).→

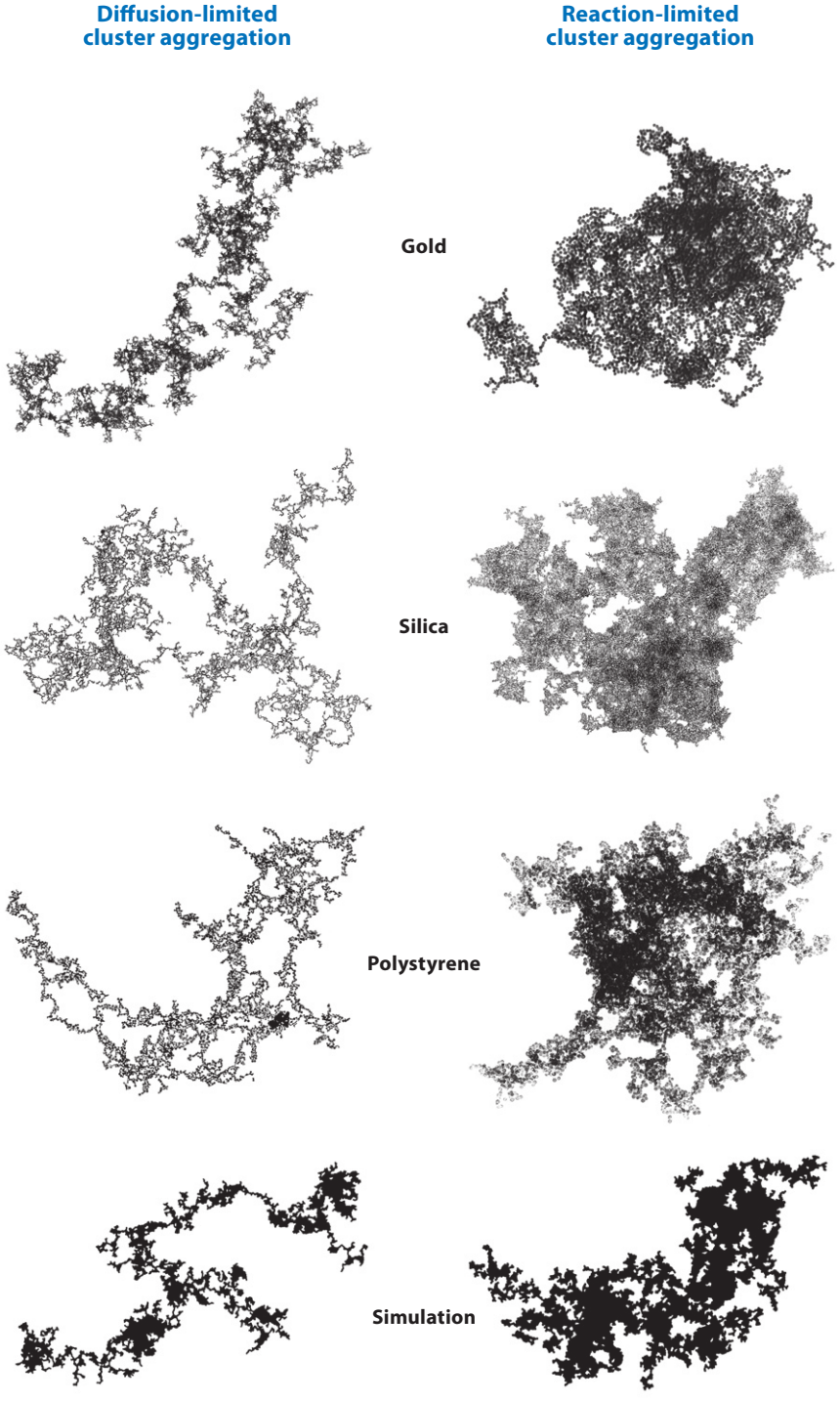

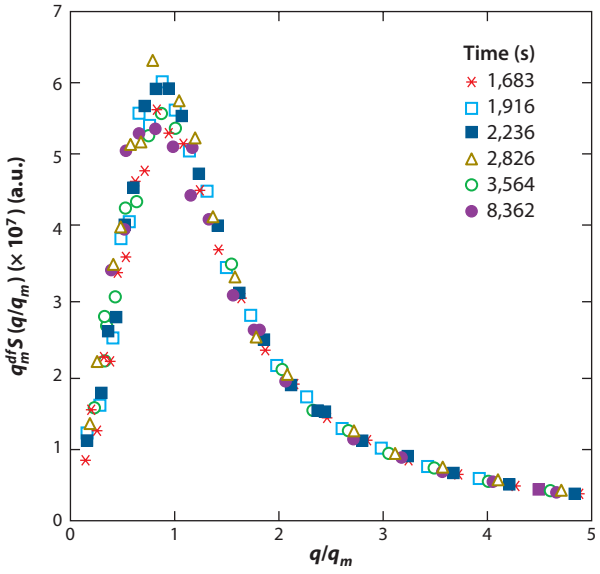

Figure 7

Normalized scaled function from light scattering data, $q_m^{df}S(q/q_m)$, as a function of normalized scattering wave vector q/q_m, for a system of 19-nm diameter polystyrene spheres at $\varphi = 2.93 \times 10^{-4}$ in a buoyancy-matched mixture of water and heavy water. Different data series correspond to measurements at different times during the later stages of a diffusion-limited cluster aggregation process. The data at different times all collapse onto a single master curve, for $d_f = 1.9 \pm 0.02$; a similar scaling is observed for samples undergoing spinodal decomposition, but with $d_f = 3$ (31).

samples with different values of φ, ξ, and concentration of polymer depletant c_p, which determines U, were created and observed, as shown in **Figure 9** (3).

Short-ranged attractions ($\xi \leq 10\%$) are particularly convenient for these studies, as simulations have found in this limit that the exact shape of the potential does not matter; instead, the integral over the potential, expressed as a normalized second virial coefficient B_2^*, controls the behavior of the system (32). This potential-shape independence allows the reconstruction of simulated data sets with the exact same behavior as the experimental systems, from which exact thermodynamic parameters, in particular B_2^* for each φ and c_p, can be determined. By using simulation to extract these parameters from the behavior of the experimental system, the experimental systems can be mapped directly onto existing theoretical frameworks; this quantitative mapping facilitates comparison, for instance, where a given sample falls relative to calculated phase-separation boundaries. In particular, the experimental observation of the onset of gelation at an experimentally well-defined gelation line maps exactly onto the theoretically predicted phase-separation boundary (4, 33). That is, it is an equilibrium thermodynamic phenomenon, spinodal decomposition, that drives the formation of colloidal gels (34); previously, these gels were generally thought to have been a purely kinetic phenomenon, though the connection with thermodynamic phase separation was anticipated by the earlier comparison between DLCA and spinodal clusters (31). The detailed comparison between experimental colloidal systems and simulation allows for extraction of meaningful, quantitative thermodynamic parameters, permitting a much closer comparison with theory and demonstrating the power of colloidal model systems to investigate fundamental physics.

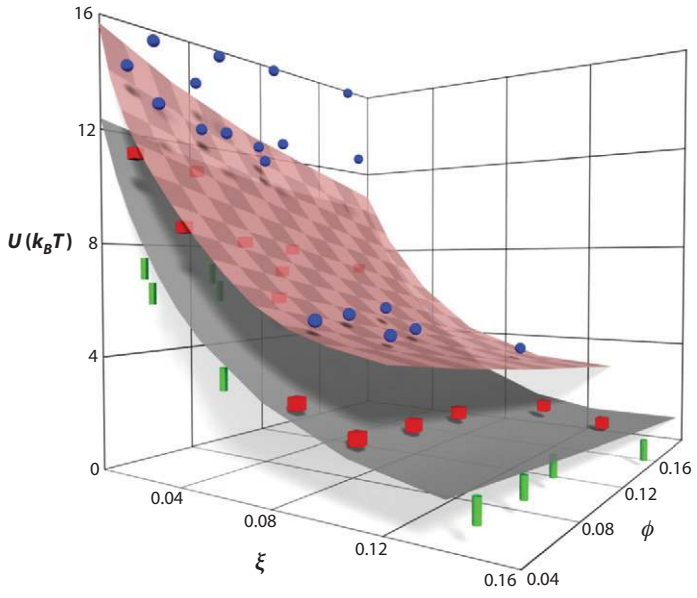

Figure 8

U-φ-ξ state diagram for colloid-polymer mixtures. Symbols represent the three phases observed with confocal microscopy: gel (*sphere*), fluids of clusters (*cube*), and monomeric fluid (*cylinder*). Surfaces are guides for the eye: Gels are above the checkered surface; monomeric fluids are below the plain surface; fluids of clusters are in between (3).

Weakly attractive colloidal particles also can be mapped onto another widely discussed phase behavior, that of jamming (35, 36), as shown in the general phase diagram in **Figure 10**. This mapping is best accomplished using the rheological properties of such suspensions, which exhibit a remarkable scaling behavior: the viscoelastic moduli scale onto a single, universal master curve (37). To illustrate this, viscoelastic moduli were examined as functions of frequency for a series of colloidal gels, made from weakly attractive carbon black samples suspended in oil. The elastic modulus, $G'(\omega)$, is always greater than the viscous modulus, $G''(\omega)$, reflecting the solid-like behavior of the samples, as shown in **Figure 11*a***. The elastic modulus is nearly independent of frequency, and its value increases sharply with volume fraction. All the data can be scaled onto a single master curve, as shown in **Figure 11*b***. The scaling arises because the rheological response consists of a combination of the solid-like contribution from the spanning colloidal network and the fluid-like contribution of the background fluid. As the particle volume fraction or interaction potential between the particles changes, the fluid-like contribution remains essentially fixed, while the solid-like contribution changes with both the volume fraction and the interaction potential. The viscoelastic response is approximately the sum of the two contributions, and thus to scale one set of data onto another, the data in **Figure 11*a*** must be shifted in the $\hat{y}$-direction to reflect the changed contribution of the solid-like portion of the solid, while the data must be shifted in $\hat{x}$-direction to reflect the change in the crossover between elastic and viscous behavior. Doing this requires the data to be shifted along a diagonal, and this accounts for the scaling observed in **Figure 11*b***.

The advantage of scaling the data onto this master curve is that it enables the precise determination of the contribution of the elastic, solid-like component, even when the sample is too

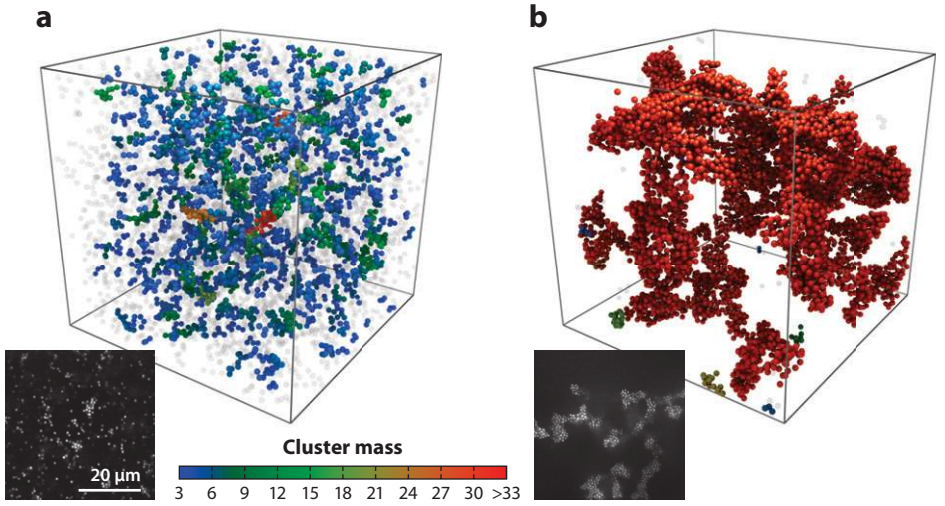

Figure 9

(*a*) 3D reconstruction ($56 \times 56 \times 56\ \mu m^3$), and (*inset*) single 2D confocal microscope image, for the fluid with the $c_p = 3.20\ mg\ ml^{-1}$. The fluid's clusters are colored by their mass (number of particles) according to the color bar, with monomers and dimers rendered in transparent gray to improve visibility. (*b*) Reconstruction and confocal image of the gel with $c_p = 3.31\ mg\ ml^{-1}$ shown at the same scale, containing a single spanning cluster (4).

weak to directly access it with the rheometer. This makes it possible to measure the dependence of the elastic component near the liquid-solid transition, and it exhibits a power-law dependence similar to rigidity percolation (38). These data can also be combined to describe the solid-to-fluid

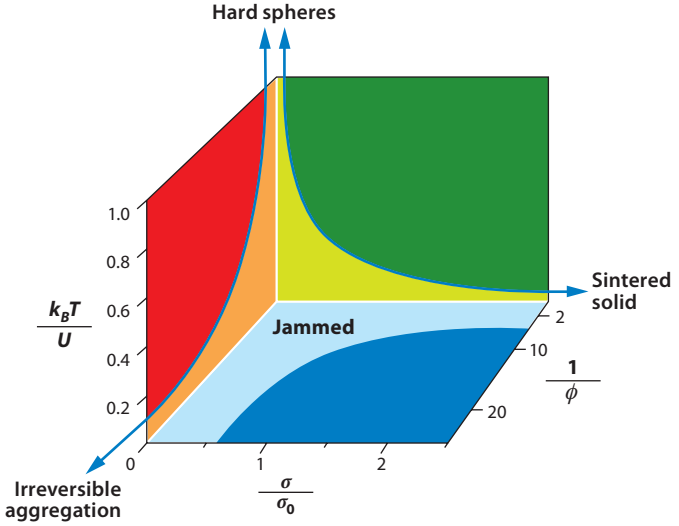

Figure 10

Composite jamming phase diagram for attractive colloidal particles, focusing on $k_BT/U \leq 1$ and $\varphi \leq 0.5$ and thus not considering the limits of true hard spheres or of very high concentrations, where more complex behavior with increasing σ may occur. Data from the three different colloid systems—carbon black, polymethylmethacrylate, and polystyrene—are used to construct this phase diagram (36).

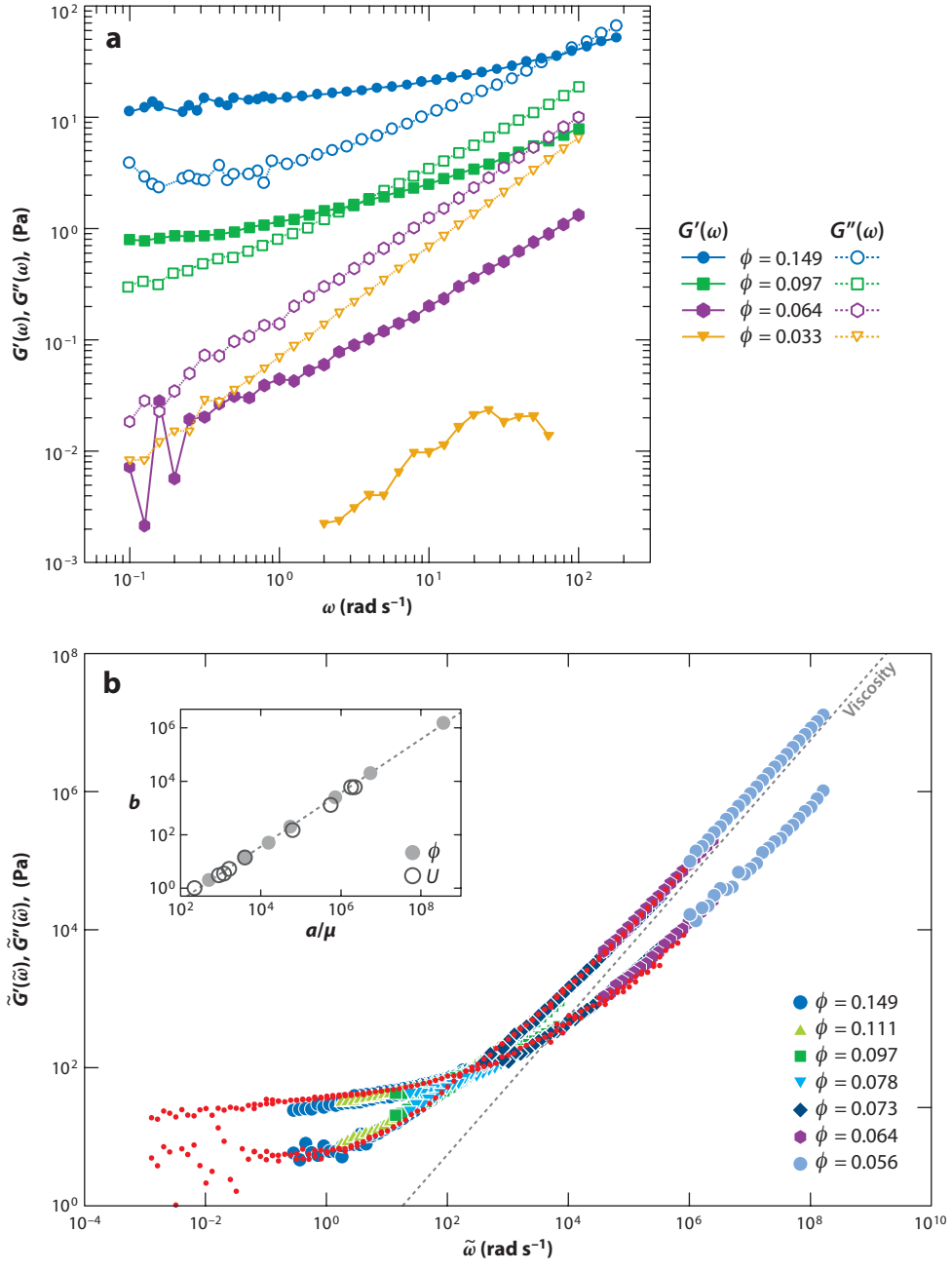

Figure 11

(*a*) $G'(\omega)$ (*filled symbols*) and $G''(\omega)$ (*open symbols*) for three different volume fractions of carbon black in the solid-like regime, with $\varphi =$ 0.149 (*circles*), 0.097 (*squares*), and 0.064 (*hexagons*) from top to bottom, and in the fluid-like regime for $\varphi = 0.033$, shown by the filled [$G'(\omega)$] and open [$G''(\omega)$] orange triangles. (*b*) Master curve showing the scaled moduli for different ϕ (*filled symbols*) and U (*red dots*) as functions of the scaled frequency. The dashed gray line represents the viscosity of the oil. The inset shows the linear relationship between the scaling factors, b and a/μ, for ϕ (*solid symbols*) and U (*open symbols*) (37).

transition phase behavior as a function of U/k_BT and φ. Moreover, shear disrupts the structure, causing the solid-like structure to become fluid like. This is analogous to the jamming transition, and it is possible to map the properties of the solid-to-fluid transition for this system onto the behavior predicted for jamming (36). Indeed, this was the earliest experimental observation of jamming.

6. CONCLUSION

This article presents a brief review of colloidal particles interacting in three different manners: as crystals, as glasses, and as gels. In each case, the behavior of the colloidal suspension exhibits fascinating phenomena and provides new insights about the phase behavior of more traditional materials, where the individual colloidal particles can model the properties of atoms or molecules. In contrast with atomic and molecular systems, both the position and the dynamics of each colloidal particle can be tracked in time, providing much greater insight about both the colloidal suspension and, consequently, about other more general systems, as well. The exquisite control over the size, materials, and interparticle interactions that can be achieved with colloidal particles makes them an excellent model system that continues to unearth new physics.

DISCLOSURE STATEMENT

The authors are not aware of any affiliations, memberships, funding, or financial holdings that might be perceived as affecting the objectivity of this review.

ACKNOWLEDGMENT

We gratefully acknowledge funding from NASA (NNX08AE09G, NNX08AE09G S11, NNC08BA08B), the NSF (DMR-1006546), and the Harvard MRSEC (DMR-0820484).

LITERATURE CITED

1. Pusey PN, van Megan W. 1986. *Nature* 320:340–42
2. Pusey PN, van Megan W. 1987. *Phys. Rev. Lett.* 59:2083–86
3. Lu PJ, Conrad JC, Wyss HM, Schofield AB, Weitz DA. 2006. *Phys. Rev. Lett.* 96:028306
4. Lu PJ, Zaccarelli E, Ciulla F, Schofield AB, Sciortino F, Weitz DA. 2008. *Nature* 453:499–503
5. Hsu MF, Dufresne ER, Weitz DA. 2005. *Langmuir* 21:4881–87
6. Pieranksi P. 1980. *Phys. Rev. Lett.* 45:569–72
7. Pieranksi P, Strzelecki L, Pansu B. 1983. *Phys. Rev. Lett.* 50:900–3
8. Williams R, Crandall RS, Wojtowicz PJ. 1976. *Phys. Rev. Lett.* 37:348–51
9. Palberg T, Haertl W, Wittig U, Versmold H, Wuerth M, Simnacher E. 1992. *J. Chem. Phys.* 96:8180–83
10. Gasser U, Weeks ER, Schofield A, Pusey PN, Weitz DA. 2002. *Science* 292:258–62
11. Leunissen ME, Christova CG, Hynninen A-P, Royall CP, Campbell AI, et al. 2005. *Nature* 437:235–40
12. Sirota EB, Ou-Yang HD, Sinha SK, Chaikin PM. 1989. *Phys. Rev. Lett.* 62:1524–27
13. Schall P, Cohen I, Weitz DA, Spaepen F. 2004. *Science* 305:1944–48
14. Pusey PN, van Megan W, Bartlett P, Ackerson BJ, Rarity JG, Underwood SM. 1989. *Phys. Rev. Lett.* 63: 2753–56
15. van Blaaderen A, Ruel R, Wiltzius P. 1997. *Nature* 385:321–24
16. Schall P, Cohen I, Weitz DA, Spaepen F. 2006. *Nature* 440:319–23
17. Mason TG, Weitz DA. 1995. *Phys. Rev. Lett.* 75:2770–73
18. Conrad JC, Dhillon PD, Weeks ER, Reichman DR, Weitz DA. 2006. *Phys. Rev. Lett.* 97:265701
19. Weeks ER, Weitz DA. 2002. *Phys. Rev. Lett.* 89:095704

20. Weeks ER, Crocker JC, Levitt AC, Schofield A, Weitz DA. 2000. *Science* 287:627–31
21. Schall P, Weitz DA, Spaepen F. 2007. *Science* 318:1895–99
22. Falk ML, Langer JS. 1998. *Phys. Rev. E* 57:7192–205
23. Falk ML, Langer JS. 2011. *Annu. Rev. Condens. Matter Phys.* 2:353–73
24. Manning ML, Langer JS, Carlson JM. 2007. *Phys. Rev. E* 76:056106
25. Shi YF, Katz MB, Li H, Falk ML. 2007. *Phys. Rev. Lett.* 98:185505
26. Mattsson J, Wyss HM, Fernandez-Nieves A, Miyazaki K, Hu Z, et al. 2009. *Nature* 462:83–86
27. Pham KN, Puertas AM, Bergenholtz J, Egelhaaf SU, Moussaid A, et al. 2002. *Science* 296:104–6
28. Weitz DA, Oliveria M. 1984. *Phys. Rev. Lett.* 52:1433–36
29. Weitz DA, Huang JS, Lin MY, Sung J. 1985. *Phys. Rev. Lett.* 54:1416–19
30. Lin MY, Lindsay HM, Weitz DA, Ball RC, Klein R, Meakin P. 1989. *Nature* 339:360–62
31. Carpineti M, Giglio M. 1992. *Phys. Rev. Lett.* 86:3327–30
32. Noro MG, Frenkel D. 2000. *J. Chem. Phys.* 113:2941–44
33. Zaccarelli E, Lu PJ, Ciulla F, Weitz DA, Sciortino F. 2008. *J. Phys. Condens. Matter* 20:494242
34. Foffi G, De Michele C, Sciortino F, Tartaglia P. 2005. *Phys. Rev. Lett.* 94:078301
35. Liu AJ, Nagel SR. 1998. *Nature* 396:21–22
36. Trappe V, Prasad V, Cipelletti L, Segre PN, Weitz DA. 2001. *Nature* 411:772–75
37. Trappe V, Weitz DA. 2000. *Phys. Rev. Lett.* 85:449–52
38. Feng SC, Sen PN, Halperin BI, Lobb CJ. 1984. *Phys. Rev. B* 30:5386–89

Annual Review of Condensed Matter Physics

Volume 4, 2013

Contents

Errata

An online log of corrections to *Annual Review of Condensed Matter Physics* articles may be found at http://conmatphys.annualreviews.org/errata.shtml